Springer

KSME

Journal of Mechanical Science and Technology 24 (9) (2010) 1875~1883
www.springerlink.com/content/1738-494x
DOI 10.1007/s12206-010-0603-1

An automated CAE system for multidisciplinary structural design : its application to micro accelerometer †

Joon-Seong Lee[1,*] and Ho-Jung Lee[2]

[1]*Dept. of Mechanical System Engineering, Kyonggi University, San 94-6, Iui-dong, Yeongtong-gu, Suwon, 443-760, Korea*
[2]*Graduate School of Mechanical Engineering, Kyonggi University, San 94-6, Iui-dong, Yeongtong-gu, Suwon, 443-760, Korea*

(Manuscript Received December 14, 2009; Revised March 19, 2010; Accepted May 4, 2010)

Abstract

This paper describes a new computer-aided engineering system for multidisciplinary structural design. An automatic finite element mesh generation technique, based on fuzzy knowledge processing and computational geometry, is incorporated into the system, together with one of the commercial finite element analysis codes. A bubble is generated if its distance from existing bubble points is similar to the bubble-spacing function at the point. The bubble-spacing function is well controlled by fuzzy knowledge processing. The Delaunay method is employed as a basic tool for element generation. Automatic finite element generation for three-dimensional MEMS holds great benefits for analyses. An optimum design solution or satisfactory solutions will be automatically searched using the genetic algorithms modified for real search space, together with the automated finite element analysis system. A novel CAE system was developed, and successfully applied to the shape design of a micro accelerometer based on a tunneling current concept.

Keywords: Delaunay triangulation; Bubble packing; Fuzzy knowledge processing; Automatic mesh generation

1. Introduction

Nuclear-reactor structural components such as pressure vessels and piping are typical examples of very-large-scale artifacts; micromachines, contrastingly, are typical examples of very-small-scale artifacts. Micromachine artifacts are extremely novel, and boast a variety of special characteristics. Utilizing their tiny dimensions ranging roughly from 10μm to 10^3μm, micromachines can perform tasks that would be impossible for conventional artifacts [1]. The design of micromachines is (a) multi-disciplinary, (b) strongly interactive among design subprocesses including design specification, conceptual design and detailed design, and (c) requires a designer dealing with the microscopic world to have the very unique empirical knowledge that is valid there. Micromachines have to be designed and evaluated in consideration of the coupled physical phenomena to which they are related. Much trial and error then, is indispensable. Such situations make it very difficult to find a satisfactory or optimized solution for practical structures such as micromachines, though numerous optimization algorithms have been studied [2].

Numerical simulation methods such as the finite element (FE) method, products of the dramatic strides made in computer technology, are recognized as key tools for practical design and analysis. Computer simulations allow for relatively quick and easy testing of new designs and iterative optimization of existing designs. And computer simulation is particularly essential to micromachine design, given the great difficulty of measuring and analyzing physical phenomena in the microscopic realm. Unfortunately, conventional computational analysis of micromachines remains labor-intensive, and is especially challenging for ordinary designers and engineers, who are obliged to find satisfactory optimized solutions, utilizing conventional computer simulations tools.

SENSIM [3], FastCap [4], MEMCAD [5] and CAEMEMS [6] are the CAD/CAE systems that have been developed for micromachines thus far. SENSIM allows for the modeling of silicon piezoresistive or capacitive pressure sensors of multiple thin films, and for the calculation of their stress and deflection as a function using finite different solutions. FastCap is a boundary element analysis program, and MEMCAD is an integrated CAD system incorporating structure generation software. CAEMEMS enables parametric modeling of devices, employing one of the commercial FE codes, ANSYS. One module of CAEMEMS is specially developed for the diaphragm of pressure sensors. In these systems, FE codes for simulation of micromachine behaviors play very important roles. To further improve the efficiency of design processes for actual micro structures of arbitrary geometry, it is indispensa-

† This paper was recommended for publication in revised form by Associate Editor Jeong Sam Han

* Corresponding author. Tel.: +82 31 249 9813, Fax: +82 31 244 6300
E-mail address: jslee1@kyonggi.ac.kr

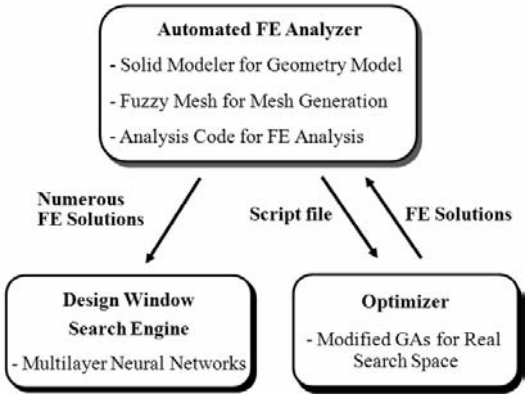

Fig. 1. System configuration.

ble that they be subject to fully automated FE modeling and analysis. In addition, CAD/CAE systems for micromachines have to possess some mechanisms to efficiently search satisfactory optimum design solutions, considering all related phenomena as well as the design requirements of micromachines.

The present authors developed a new computer-aided engineering system for multidisciplinary structural design into which an automatic FE mesh generation technique, based on fuzzy theory [7, 8] and computational geometry, together with one of commercial solid modelers, is incorporated. In the present study, to support the FE analysis system, which requires such special mesh, automatic bubble mesh generation was combined with the automatic mesh generation system. Additionally, the authors derived the concept of an automated design system for multidisciplinary phenomena, which works in conjunction with various soft-computing and intelligent simulation techniques such as neural networks and genetic algorithms (GA). This system can help to effect significant improvement in the quality of final design solutions. It was applied to the design optimization of a novel tunnel current based on a micro accelerometer.

2. Outline of system

The present system configuration is illustrated in Fig. 1. To efficiently support design processes for practical structures such as micromachines, the automatic finite element system, which is based on fuzzy knowledge processing and computational geometry techniques, is integrated with a GA. By integrating a GA-based optimizer, the system allows automatic searching for optimum design solutions. Also, the system allows for automatic generation of a multi-dimensional design window in which a number of satisfactory design solutions existing multilayer neural networks can be searched [9]. Most of the components of the present system, excepting the FE program, are constructed on personal computer using the C++ language.

2.1 Finite element analyzer

The one of the commercial geometric modelers, is em-

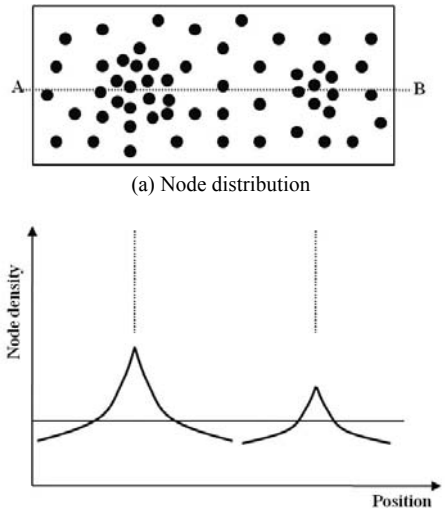

(a) Node distribution

(b) Node density function along line A-B

Fig. 2. Example of node density function.

ployed for 3D solid structures. Material properties and boundary conditions are directly attached to the geometric model by clicking the model's-loops or edges using a mouse, and then by inputting the actual values.

In the present system, nodes are first generated, and then an FE mesh is built. In general, it is not so easy to effectively control element size for a complex geometry. An example of the node density function [7] is shown in Fig. 2. A node density distribution over an entire geometric model is constructed as follows. The present system stores several local node patterns, such as the pattern suitable to capture stress concentration, the pattern to subdivide a finite domain uniformly, and the pattern to subdivide a whole domain uniformly. A user selects some of those local node patterns, on the basis of their analysis purposes, and designates their relative importance and location.

Node generation is a time-consuming process in automatic mesh generation. In the present study, bubble meshing [8] was adopted to generate nodes satisfying the node density distribution over the entire analysis domain.

Bubble meshing can be summarized as a two step sequence: (1) packing circles or spheres, called bubbles, closely in a domain; (2) connecting their centers by Delaunay triangulation, which, avoiding small angles, selects the best topological connections for a set of nodes.

2.1.1 Bubble packing

The key element of bubble meshing lies in the first step, that is, the optimization of mesh node locations by close packing bubbles. By this method, bubbles move in a domain until forces between them are stabilized, and Delaunay triangulation is then applied to generate a mesh connecting the nodes defined by the bubble packing. A repulsive or attractive force much like an intermolecular van der Waals force is assumed to exist between two adjacent bubbles. A globally stable configuration of tightly packed bubbles is determined by solving

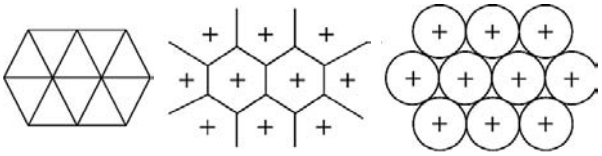

(a) Delaunay triangulation (b) Voronoi polygons (c) Packed bubbles

Fig. 3. Schematics of Delaunay triangulation, Voronoi polygons, and packed bubbles.

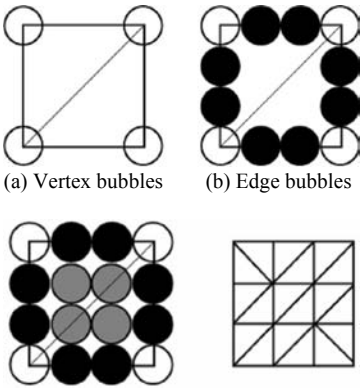

(a) Vertex bubbles (b) Edge bubbles

(c) Loop bubbles (d) Final mesh

Fig. 4. Bubble mesh procedure.

the equation of motion. The novelty of this method is that the close packing of bubbles forms a pattern of Voronoi polygons, corresponding to well-shaped Delaunay triangles. Fig. 3 shows this relationship for a uniform node-spacing case. Fig. 4 shows the procedure of the bubble packing method. Bubble meshing generates a two-dimensional triangular mesh (a) solving the equation of motion on vertices, edges, and faces (or loops), in that order, and (b) generating a triangular mesh by connecting the center points of the bubbles by Delaunay triangulation. Similar steps are applied to the generation of three-dimensional tetrahedral meshes. In this procedure, the mesh density is needed in order to determine the radius of the bubbles. To handle general bubble spacing, we adopted bubble density distribution function.

2.1.2 Dynamic bubbles

A force function f(r) between two adjacent bubbles is shown in Fig. 5.

If $f(r)=r_0$, r_0 is defined as

$$r_0 = 0.5(d_i + d_j) \tag{1}$$

where d_i, d_j denote the diameters of two adjacent bubbles.

The two bubbles are defined as being at a stable distance. If $f(r)$ is larger than zero, a repulsive force is assumed to exist between the two bubbles, and if $f(r)$ is smaller than zero, an attractive force is assumed to exist between them. The kinetic equation is written as follows:

$$m_i \frac{d^2 s_i}{dt^2} + c\frac{ds_i}{dt} = f_i, \qquad i = 1, 2, ..., n. \tag{2}$$

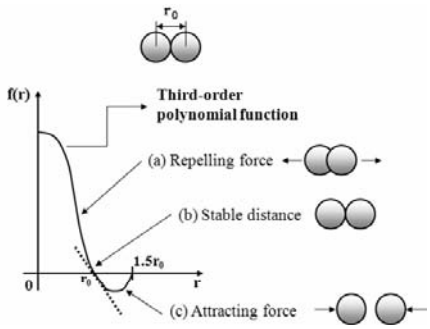

Fig. 5. Interbubble proximity-based forces.

where m_i denotes the mass of a bubble, c the coefficient of viscosity, s_i the position vector of the bubble center, n the total number of bubbles and f_i the resultant force acting on the i-th bubble. The system of Eq. (2) describes the process of physical relaxation, which eventually moves the bubbles to their proper equilibrium positions. The force f_i, which depends on the position x_i and the distances from its center to the centers of the neighboring bubbles, is modeled by the van der Waals force. Let r denote the distance between the centers of two adjacent bubbles. Then, van der Waals reactions on the bubbles, as shown in Fig. 5, are approximated by the 3rd-order polynomials [10]:

$$f(r) = \begin{cases} ar^3 + br^2 + cr + d, & 0 \le r \le 1.5r_0 \\ 0, & r < 0,\ \ 1.5r_0 < r \end{cases} \tag{3a}$$

$$f(r_0) = 0,\ f(1.5\,r_0) = 0,\ f'(0) = 0,\ f'(r_0) = -k_0 \tag{3b}$$

where $f(r)$ indicates the magnitude of the force between the two neighboring bubbles, and k_0 is the linear elastic constant at the equilibrium distance r_0. Note that the force at $r = 0$ is not infinite in this model, and the forces are activated within a limited distance ($r<1.5\,r_0$). The finite force at $r = 0$ prevents a singular case in which the centers of bubbles coincide with each other. To reduce the calculation time, only the bubbles within a limited distance ($r<1.5\,r_0$) are considered in the present bubble packing method.

The initial forces $f_i(r)$ are defined from the initial bubbles, and the final positions should be determined by enforcing the system of Eq. (2) via iteration until the equilibrium state is reached, i.e.,

$$f_i = 0\ (i = 1, 2, ..., n). \tag{4}$$

We employ the 4th-order Runge-Kutta method to solve the system of Eq. (2). In this way, the optimized bubble configuration is obtained. In the process of the optimization, the population of bubbles is adaptively controlled using the fuzzy knowledge process. That is, excess bubbles that significantly overlap their neighbors are removed, and new bubbles are added around open bubbles that lack the appropriate number of neighboring bubbles. After the optimization of the bubble configuration, a triangular mesh is generated by Delaunay triangulation.

2.1.3 Control of bubble patterns by fuzzy knowledge

In this section, the process of connecting locally optimum bubble images is dealt with using the fuzzy knowledge processing technique. Performances of automatic mesh generation methods based on node generation algorithms depend on how node spacing functions or node density distributions are controlled, and on how nodes are generated. The basic concept of the present mesh generation algorithm originates from the imitation of mesh generation processes conducted by human experts using finite element analyses. One of the aims of this algorithm is to make such experts' techniques accessible to beginners.

In the present method, field A close to the hole and field B close to the crack-tip are defined in terms of the membership functions used in the fuzzy set theory. In practice, the membership function can be expressed as μ (x, y) in this particular example, and in 3D cases it is a function of 3D coordinates, i.e. μ (x, y, z). This procedure of node generation, i.e. the connection procedure for both node patterns, is summarized as follows :

· If $\mu_A (x_p, y_p) \geq \mu_B (x_p, y_p)$ for a node p (x_p, y_p) belonging to pattern A, then node p is generated; otherwise p is not generated.

· If $\mu_A (x_q, y_q) \geq \mu_B (x_q, y_q)$ for a node q (x_q, y_q) belonging to pattern B, then node q is generated; otherwise q is not generated.

It is apparent that the above algorithm can be easily extended to 3D problems and any number of node patterns. In addition, since finer node patterns are generally required to be placed near stress concentration sources, it is convenient to let the membership function correspond to bubble density as well.

2.1.4 Element generation

The Delaunay triangulation method [11,12] is utilized to generate tetrahedral elements from numerous bubbles given in a geometry. The speed of element generation by the this method is proportional to the number of nodes.

In this system, after all of the bubbles are generated in the analysis domain and on its boundary, the system creates triangular (in 2D) or tetrahedral (in 3D) elements.

If this method is utilized to generate elements in a geometry of indented shape, elements are inevitably generated even outside the geometry. However, such mis-matched elements can be removed by performing the IN / OUT check [13] to determine their gravity center points. In addition, it is necessary to avoid the generation of those mis-matched elements crossing domain boundaries, by setting the node densities on the edges slightly higher than those inside the domain near the boundaries.

2.2 Design window search engine

The Design Window (DW) is a schematic drawing of an area for satisfactory solutions in a permissible multi-dimensional design parameter space. The DW seems more useful in practical situations than one optimum solution determined under limited consideration. Among several algorithms, the Whole-area Search Method (WSM) is employed here. As shown in Fig. 6, a lattice is first generated in the design parameter space empirically determined by a user. All of the lattice points are then examined one by one to determine whether they satisfy the design criteria or not. The WSM is the most flexible and robust, but the number of lattice points to be examined tends to be extremely large. Therefore, the present authors used a novel method to efficiently search the DW using the multilayer neural network [9].

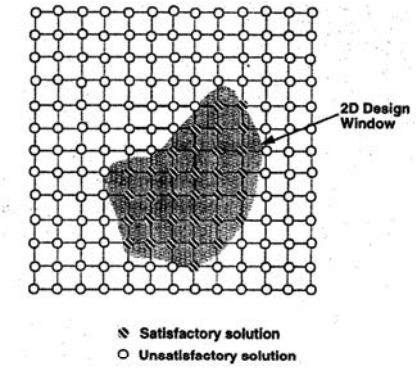

Fig. 6. Design Window in 2D parameter space.

This method consists of three subprocesses. First, using the automated FE system, numerous FE analyses are performed to prepare training data sets and test data sets for the neural network, each of which is a coupled data set of assumed design parameters vs. calculated physical values. The neural network is then trained using the training data sets. Here the design parameters assumed are given to the input units of the network, while the physical values calculated are shown to the output units as teacher signals. A training algorithm employed here is backpropagation.

After a sufficient number of training iterations, the neural network can imitate a response of the FE system. That means, the well trained network provides some appropriate physical values even for unknown values of design parameters. Finally a multi-dimensional DW is immediately searched using the well trained network together with the WSM.

2.3 Modified GA

In optimum or satisfactory design problems of modern artifacts such as nuclear-reactor structural components, electronic devices and micromachines, GAs, have attracted much attention, having been applied to various inverse problems and optimum designs [14]. For continuous search space problems, conventional GAs, however, tend to converge slowly, and their accuracy can strongly depend on the bit length of the binary code employed. Therefore, the present authors proposed a new GA modified for the real search space [15], and

```
k = 0
Initialize P(k);
k = k + 1
do
    Recombine P(k);
    Mutate P(k);
    Evalute P(k);
    Select P(k);
While terminal conditions is nat satisfied
```

Fig. 7. Fundamental structure of Gas.

this formulation was used as an optimization engine.

The fundamental structure of the GA is shown in Fig. 7. First, a population of individuals, each represented by a vector, is generated initially (generation t=0) at random, i.e.,

$$P(k)=|u_1(k), ...,u_\lambda \in (k)| \in \mathbf{I}^\lambda \tag{5}$$

where $\lambda \in \mathbf{N}$ and $\mathbf{I}$ represent the population size of the parental individuals and the space of an individual respectively. The population then evolves towards better regions of the search space by means of randomized processes of recombination, mutation and selection though either the recombination or the mutation operator is not implemented in some algorithms. In the recombination operator $\mathbf{r} : \mathbf{I}^\lambda \rightarrow \mathbf{I}^\gamma$, λ parental individuals breed γ ($\in \mathbf{N}$) offspring individuals by combining parts of the information from the parental individuals. The mutation $\mathbf{m} : \mathbf{I}^\gamma \rightarrow \mathbf{I}^\lambda$, then, forms new individuals by making large alterations to the offspring individuals regardless of their inherent information. In the evaluation of the fitness of all of the individuals, the selection operator $\mathbf{s} : \mathbf{I}^\gamma \cup \mathbf{I}^{\gamma+\lambda} \rightarrow \mathbf{I}^\lambda$ favorably selects individuals of higher fitness to produce more often than those of lower fitness. These reproductive operations from one generation in the evolutionary process, which corresponds to one iteration in the algorithm, and the iteration is repeated until a given terminal criterion is satisfied.

Selection in canonical genetic algorithms emphasizes a probabilistic survival rule mixed with a fitness dependent chance to have different partners for producing more or less spring. By deriving an analogy to the game-theoretic multi-armed bandit problem, Holland identifies a necessity to use proportional selection in order to optimize the trade-off between further exploiting promising regions of the search space while at the same time also exploring other regions [16]. For proportional selection $\mathbf{S} : \mathbf{I}^\lambda \rightarrow \mathbf{I}^\lambda$, the reproduction probabilities of individuals u_i are given by their relative fitness, i.e. $i \in \{1, ..., \lambda\}$:

$$P_s\left(u_i^k\right) = \frac{\Phi\left(u_i^k\right)}{\sum_{j=1}^{\lambda} \Phi\left(u_i^k\right)} \quad . \tag{6}$$

Sampling λ individuals according to this probability distribution yields the next generation of parents.

Table 1. Internal parameters for both algorithms.

	Canonical GA	Modified GA
Population size	50	50
Bit length per variable	30	-
Crossover rate	0.95	-
Mutation rate	0.001	-
Standard deviation	-	0.5 (constant)
Generation gap	5	5

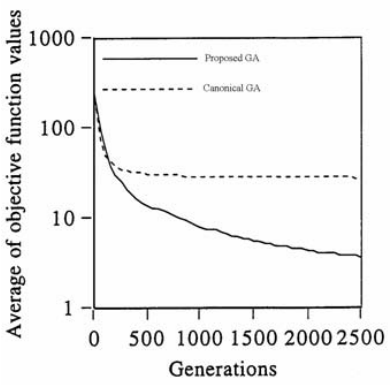

Fig. 8. Average of objective function values vs. generations.

The mathematical characteristic of the test function is unimodal. The test function is as follows:

$$\begin{aligned} &f_1(x) = \sum_{i=1}^{n} x_i^2, \quad x \in R^n; \quad n = 30, \\ &-5.12 \le x_i \le 5.12, \; x^* = [0, ..., 0)]^T, \\ &f_1(x^*) = 0. \end{aligned} \tag{7}$$

The function is the simplest quadratic function, which is characterized also by unimodality, continuity and convexity. It is often used as the test case of nonlinear functions, since many objective functions formulated in reality take this form.

The internal parameters selected for both the algorithms are listed in Table 1. The crossover and mutation rates in the canonical genetic algorithm, 0.6 and 0.001, are typically used in many studies. The standard deviation of the proposed algorithm was set to be constant, for simplicity. All of the other internal parameters were set identically for the two algorithms. For generality, ten runs were performed for each test, and the average performance of each algorithm was recorded.

The results of the search performances of the two algorithms to 2,500 generations are shown in Fig. 8. The real line indicates the outcome from the proposed method, whereas the broken line represents the outcome by the canonical genetic algorithm. The results clearly reflect the superiority of the proposed algorithm in unimodal function optimization.

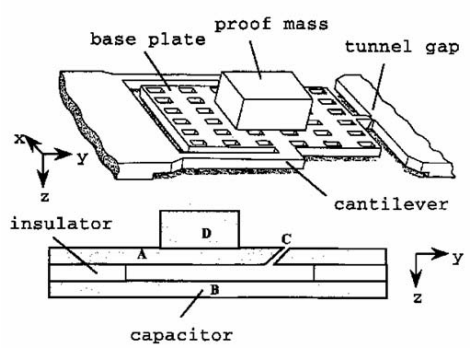

Fig. 9. Concept of micro accelerometer.

3. Design of micro accelerometer

3.1 Operation principles

The present system was applied to a novel, tunneling current-based micro accelerometer [17]. The cross-section of the device is shown in Fig. 9. In the fabrication process, bonded silicon on the insulator is used as the starting material. The proof mass is a 3 ㎛ thick Si cantilever (A) suspended 4 ㎛ above the Si substrate (B), and there is a 200 *n*m-wide gap (C) to about 2 *n*m until tunneling occurs. Added mass (D) is necessary to obtain the required sensitivity of the accelerometer, and it can be bonded to the plate using the surface-activated bonding technology.

At the beginning of the design, we made a list of possible physical effects that translate an acceleration into any measurable quantity. The list includes the change of an electric resistance caused by deflection, the induction of a voltage by a motion of a coil, the change of a capacitance, the piezoelectric effect, and the tunnel current effect. The resistance, the piezoelectric, and capacitance concepts have been tested by other groups, and induction was not suitable for miniaturization. Thus we decided to proceed with the tunnel current effect concept.

A cantilever with a small gap in the end was proposed for the realization of the micro accelerometer. A tunnel current that goes across the gap is observed to detect the change of the distance of the gap. The gap is created by the technique in which a focused ion beam is shone onto a suspended silicon bridge to make a cut at an angle of 45 degrees.

The cantilever is pulled down by an electrostatic force from the substrate to the position at which the gap comes to a specific distance. When the tip of the cantilever moves due to an acceleration, the amount of a tunnel current across the gap changes. The change is applied to the voltage of the capacitor, so that the gap is maintained at a constant distance. The amount of feedback is read out as an indicator of the acceleration.

The first version of the layout had a uniform cantilever, but it turned out to be too light to cause sufficient deflection. Then the cantilever was then redesigned to have a lumped mass supported by two arms at both sides.

Table 2. Design requirements for micro accelerometer.

1	Dynamic range	$f_1 > 1$ kHz
2	Mode I dominance	$f_1 \ll f_2$
3	Directivity	$d_3 \gg d_2, d_1$
4	Max. deflection	$d_3 < 2$ nm
5	Economy	Area 400μm × 400μm
6	Strength	$\sigma_{max} < \sigma_{ys}$
7	Max. applied voltage	V ≤ 15V
8	Controllability (sensitivity)	Compensation voltage per a_3= 1g, ΔV≈0.3V

* Notes; f_i : eigen frequency of mode i
d_i : z-displacement at tunnel gap for a_i=1g
a_i : acceleration in direction of x_i axis

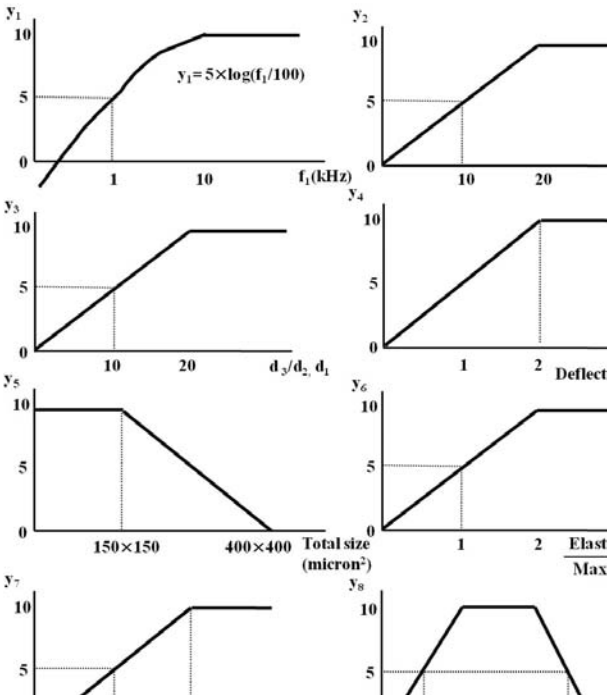

3.2 Design requirements and optimization problem

Table 2 summarizes the detailed design requirements for the present micro accelerometer. They include the dynamic and static behaviors of the device, its strength, cost and sensitivity. The purpose of the present design process was to find any structure configurations that would satisfy all of the design requirements given in Table 2. For each requirement, an empirical normalized satisfaction function was formulated. Fig. 10 shows the eight satisfaction functions of the design requirements. A score greater than 5 means that the requirement is satisfied, whereas a score of 10 means full satisfaction. The following optimization problem was formulated:

$$f(A_1, A_2, ..., A_n) = \min \{y_1, y_2, ..., y_8\} \rightarrow \max, \quad (8)$$

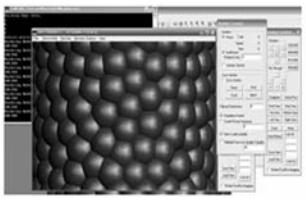

Fig. 11. Display screen of system.

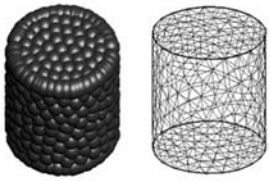

Fig. 12. Bubble image and mesh.

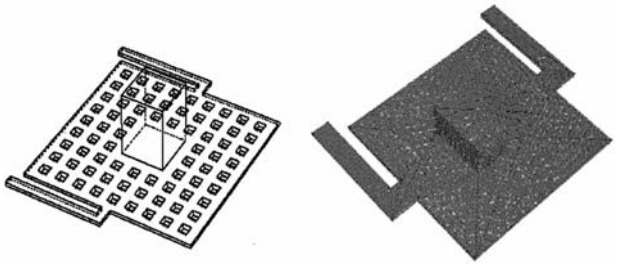

Fig. 13. Example of geometric model. Fig. 14. Bubble image of geometric model.

where A_i denotes the *i-th* design parameter specified for the problem, and y_j is a value of the satisfaction function. This problem was solved by the GAs modified for the real search space.

In this example, calculation of the fitness function was computationally expensive because it required four automatic 3D FE analyses. Therefore, computations were performed using an automated FE analyzer.

4. Results and discussions

Fig. 11 shows the system display screen, and Fig. 12 shows the uniform bubble and mesh. To demonstrate actual performances of the present system, it was applied to a micro wobble actuator and a tunneling current based micro accelerometer.

Fig. 13 shows a geometric model of the 3D accelerometer made using a solid modeler, and Fig. 14 shows the bubble image.

Fig. 15 shows a typical FE mesh, which consists of 9,042 tetrahedral quadratic elements and 19,342 nodes. Fig. 16 shows an example of stress distribution of the deformation analysis. Fig. 17 indicates the design parameters for the present micro accelerometer, and Table 3 lists their ranges. In the micro accelerometer design, knowing the dynamical behavior of the cantilever is important to determination of the dimensions. For example, the deflection of the cantilever must be large enough to be able to detect an acceleration; at the same time, the tunnel current tip must be placed in a position in which the primary or secondary oscillation modes do not interfere with the measurement.

In the GA-based optimization process, each generation consisted of 50 individuals, each one holding a vector of design parameters. Therefore, the evaluation of all individuals in one generation required 200 automatic 3D FE analyses. In order to decrease the calculation time, the distributed computation approach feature was effectively utilized, and calculations were performed concurrently on three personal computers. This way the calculation time was reduced to roughly 70 minutes per generation. Fig. 18 shows the objective function value versus generation for 4 and 6 variables. Additionally, Fig. 19 presents the results of the optimization process for the generation of the design parameters. Satisfactory designs were found after only several hours of calculations, with further calcula-

Table 3. Design parameter ranges.

Parameter	Range
x1	150 ~ 400 (μm)
x2	10 ~ 100 (μm)
x3	50 ~ 350 (μm)
x4	5 ~ 50 (μm)
x5	2 ~ 20 (g/cm^3)
x6	10 ~ 50 (μm)

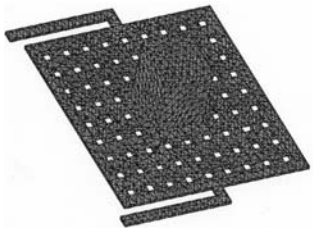

Fig. 15. Typical FE mesh.

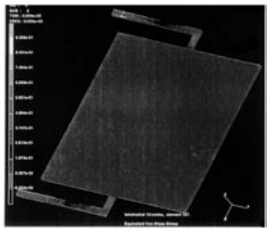

Fig. 16. Distribution of stress.

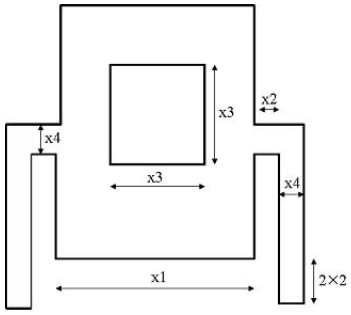

x5 : mass density of proof mass; x6 : height of proof mass

Fig. 17. Design parameters.

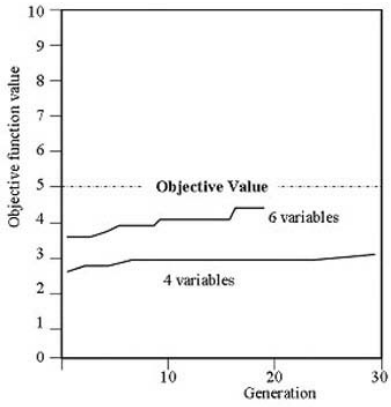

Fig. 18. Objective function value vs. generation.

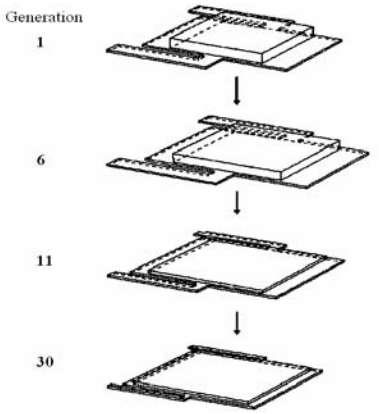

Fig. 19. Shape evolution of micro accelerometer.

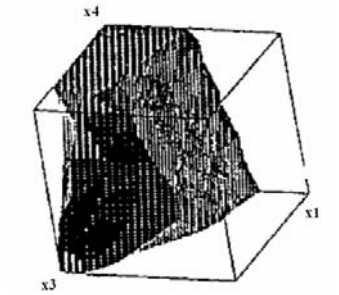

Fig. 20. Design window.

tions leading to slightly better results. Fig. 20 shows the DW in the x1, x3 and x4 spaces when x2 is 25 ㎛ and x6 ranges from 10 to 50 ㎛. The number of searched points in this DW is 18,420.

5. Conclusions

In this paper, a concept of an automated design system for multidisciplinary structural design is proposed, which, in the present study, was trialed for specific applicability using genetic algorithms. The automatic design system was built and integrated with a GA-based optimizer modified for a real search space.

An automatic mesh generation system for three-dimensional structures consisting of free-form surfaces has been presented. Several local bubble patterns were selected and automatically superposed based on the fuzzy knowledge processing technique. In addition, several computational geometry techniques were successfully applied to element generation. The developed system was utilized to generate meshes of three-dimensional complex geometry. The key features of the present algorithm are easy control of complex three-dimensional bubble density distribution with fewer input data, by means of the fuzzy knowledge processing technique, and fast node and element generation based on computational geometry techniques. The effectiveness of the present system was demonstrated through several mesh generations for three-dimensional complex geometry.

The static and dynamic deformation, vibration and electrostatic behaviors of the micro accelerometer were effectively evaluated in an easy and consistent manner using the developed system. Here, interactive operations can be performed by the user in a reasonably short time, even when solving complicated problems of 3D structures such as that of the micro accelerometer. This CAE system was successfully applied to the automated shape design of a micro accelerometer based on a tunneling current concept.

Acknowledgment

This work was carried out with financial support from the 2007 Kyonggi University specialization program.

References

[1] Y. C. Lee and J. S. Lee, FEA Simulation for Practical Behaviors of Electrostatic Micro Actuator, *J. of Korean Society of Precision Engineering*, 22 (1) (2005) 115-121.

[2] Y. Massim, A. Zeblah, R. Meziane, M. Benguediab and A. Ghouraf, Optimal Design and Reliability Evaluation of Multi-State Series-Parallel Power Systems, *Nonlinear Dynamics*, 40 (4) (2005) 309-321.

[3] K. W. Lee and K. D. Wise, SENSIM: A Simulation Program for Solid-State Pressure Sensors, *IEEE Transactions on Electron Devices*, ED-29 (1982) 34-41.

[4] K. Nabors, S. Kim, J. White and S. Senturia, *FastCap User's Guide*, Research Laboratory of Electronics, Dept. of Electrical Engineering and Computer Science, MIT, Cambridge, MA 02139, USA.

[5] J. R. Gilbert, P. M. Harris, D. O. Ouma, X. Cai, A. Pfajer, J. White and S. D. Senturia, Implementation of a MEMCAD System for Electrostatic and Mechanical Analysis of Complex Structures from Mask Descriptions, *Proceedings of the IEEE Micro Electro Mechanical Systems Workshop*, Fort Lauderdale (1993) 207-212.

[6] S. Crary, O. Juma and Y. Zhang, Software Tools for Designers of Sensors and Actuator CAE Systems, *IEEE Solid-State Sensors and Actuators*, San Francisco, USA (1991) 498-501.

[7] Y. C. Lee, J. S. Lee, Y. J. Choi and N. Y. Kim, Automatic Mesh Generation System for Novel FEM Modeling Based on Fuzzy Theory, *Journal of Fuzzy Logic and Intelligent Systems*, 15 (3) (2005) 343-348.

[8] J. S. Lee, Y. J. Choi, E. C. Lee and H. T. Kim, Mesh Generation System for Three-Dimensional FE Analysis Simulation of Micro Actuators, *The 22nd International Technical Conference on Circuits/Systems, Computers and Communications*, (2007) 903-906.

[9] D. E. Rumelhart, G. E. Hinton and G. E. Williams, Learning Representation by Back-propagation Errors, *Nature 2/e*, 323 (1986) 533-536.

[10] K. Shimada, A. Yamada and T. Itoh, Anisotropic triangular meshing of parametric surfaces via close packing of ellipsoidal bubbles, *Proceedings of 6th Int. Meshing Roundtable*, Sandia National Laboratories, (1997) 375-390.

[11] A. Fuchs, Almost Regular Delaunay Triangulations, *Int. Journal of Numerical Methods in Engineering*, 40 (1997) 4595-4610.
[12] C. K. Choi, G. H. Lee and H. J. Chung, An adaptive analysis with the element-free Galerkin method using bubble meshing technique, *Comp. Struct. Eng.*, 15 (2002) 84-95.
[13] J. S. Lee, Automated CAE System for Three-Dimensional Complex Geometry, *Doctoral Thesis*, The University of Tokyo, (1995).
[14] J. J. Grefenstette, GENESIS: A System for Using Genetic Search Procedures, *Proceedings of 1984 Conference on Intelligent Systems and Machines*, (1984) 161-165.
[15] J. S. Lee, A New Evolutionary Algorithm for Continuous Search Space, *Institute of Industrial Technology Journal*, *Kyonggi University*, To appear.
[16] R. Holland and T. A Jeeves, Direct Search Solution of Numerical and Statistical Problems, 12 (1988) 67-973.
[17] D. Moore, Micromachining and Focused Ion Beam Etching of Si for Accelerometers, *Smp. On Micro machining and Microfabrication*, SPIE, (2005).

Joon-Seong Lee received his Ph.D. degree from the University of Tokyo, Japan, in 1995. He is currently a professor in the Department of Mechanical System Engineering in Kyonggi University, Suwon South Korea. Dr. Lee's research interest is the development of an intelligent simulation system that will effectively combine numerical simulations such as those achieved by the finite element method and soft computing techniques, and its application to various artifacts such as micromachines.

Ho-Jung Lee received his B.S. degree in Mechanical System Engineering from Kyonggi University, Suwon, in 2009. He is currently there as an M.S. student in Mechanical Engineering.